MICROCOPY RESOLUTION TEST CHART

NATIONAL BUREAU OF STANDARDS-1963-A

REPORT DOCUMENTATION PAGE		READ INSTRUCTIONS BEFORE COMPLETING FORM
1. REPORT NUMBER	2. GOVT ACCESSION NO. *A133067*	3. RECIPIENT'S CATALOG NUMBER
4. TITLE (and Subtitle) Multigrid Calculation of Three-Dimensional Transonic Potential Flows		5. TYPE OF REPORT & PERIOD COVERED
		6. PERFORMING ORG. REPORT NUMBER
7. AUTHOR(s) D. A. Caughey		8. CONTRACT OR GRANT NUMBER(s) N00014-77-C-0033
9. PERFORMING ORGANIZATION NAME AND ADDRESS Cornell University Mechanical and Aerospace Engineering Ithaca, N.Y. 14853		10. PROGRAM ELEMENT, PROJECT, TASK AREA & WORK UNIT NUMBERS NR 061 - 242
11. CONTROLLING OFFICE NAME AND ADDRESS Office of Naval Research Code 438 Arlington, Virginia 22217		12. REPORT DATE January 1983
		13. NUMBER OF PAGES 9
14. MONITORING AGENCY NAME & ADDRESS(If different from Controlling Office) ONR Resident Representative 715 Broadway 5th Floor New York, N.Y. 10003		15. SECURITY CLASS. (of this report) Unclassified
		15a. DECLASSIFICATION/DOWNGRADING SCHEDULE

16. DISTRIBUTION STATEMENT (of this Report)

Approved for public release; distribution unlimited

17. DISTRIBUTION STATEMENT (of the abstract entered in Block 20, if different from Report)

18. SUPPLEMENTARY NOTES

19. KEY WORDS (Continue on reverse side if necessary and identify by block number)

Computational Fluid Dynamics
Transonic Flow
Aerodynamics

SEP 2 0 1983

E

20. ABSTRACT (Continue on reverse side if necessary and identify by block number)

    A multi-grid algorithm has been developed to speed the iterative
convergence of calculations for the transonic potential flow past swept
wings and wing-fuselage combinations. The method is based upon a fully-
conservative, finite-volume approximation to the steady potential equation
which is second-order accurate everywhere in the flow field except near
shock waves. The multi-grid scheme is incorporated within the framework
of an alternating successive-line-overrelaxation (SLOR) solver of the

83 09 28 009

difference equations. Computed results confirm the second-order accuracy
of the scheme, and demonstrate the effectiveness of the multi-grid procedure.

AIAA'83

AIAA-83-0374

Multi-Grid Calculation of Three-Dimensional Transonic Potential Flows

D.A. Caughey, Cornell Univ., Ithaca, NY

THE RUTH H. HOOKER
                              Y

           1983

NAVAL RESEARCH LABORATORY

AIAA 21st Aerospace Sciences Meeting

January 10-13, 1983/Reno, Nevada

MULTI-GRID CALCULATION OF THREE-DIMENSIONAL

TRANSONIC POTENTIAL FLOWS

D. A. Caughey[1]

Cornell University
Ithaca, New York   14853

ABSTRACT

A multi-grid algorithm has been developed to speed the iterative convergence of calculations for the transonic potential flow past swept wings and wing-fuselage combinations. The method is based upon a fully-conservative, finite-volume approximation to the steady potential equation which is second-order accurate everywhere in the flow field except near shock waves. The multi-grid scheme is incorporated within the framework of an alternating successive-line-overrelaxation (SLOR) solver of the difference equations. Computed results confirm the second-order accuracy of the scheme, and demonstrate the effectiveness of the multi-grid procedure. ⟵

I. INTRODUCTION

In the past several years, algorithms have been developed for predicting the transonic potential flow past reasonably complete aircraft configurations. In particular, the finite-volume method of Jameson and Caughey[1-3] has made it possible to calculate the transonic potential flow past any configuration for which a suitable boundary-conforming coordinate grid can be constructed. These schemes still remain quite expensive in terms of computer resources for practical use, however, primarily because of the large number of grid cells necessary for adequate resolution in three-dimensional problems and the large number of iterations required to achieve even modest convergence on these fine grids. The present paper describes work addressed primarily at this last difficulty, but also includes an improvement which addresses the first problem.

The major thrust of the current work is the incorporation of a multi-grid algorithm[4,5] to solve the difference equations. At the same time, the artificial viscosity terms have been modified to maintain almost everywhere the second-order accuracy of the original central-difference approximation used in subsonic regions of the flowfield in a manner similar to that used for two-dimensional calculations by Jameson in Reference 6. When using multi-grid to accelerate convergence in two-dimensional calculations, Jameson[7] found it necessary to use a generalized Alternating-Direction-Implicit (ADI) smoothing routine to eliminate all high wavenumber components of the error, however the results of Shmilovich and Caughey[8] and their extension to the current work demonstrates that good rates of

convergence can be obtained using modified versions of the original SLOR algorithms. In order to provide reliable convergence, the bandwidth of the original SLOR scheme has been increased to allow pentadiagonal inversions along each line (instead of the tridiagonal inversions of the original scheme).

In the present paper, a brief review of the fully-conservative finite volume scheme will first be presented, concentrating upon those aspects necessary for an understanding of the improvements in the artificial viscosity, the modified SLOR schemes, and the implementation of the multi-grid algorithm. The changes resulting from the implementation of the new features will then be described, and results indicating the improved iterative convergence and accuracy of the new scheme will be presented. A comparison of results calculated using the original first-order accurate and new second-order accurate schemes will also provide some guidelines on the number of mesh points required for given levels of accuracy in force coefficients for these three-dimensional calculations.

II. ANALYSIS

The current work is based upon the finite-volume method of Jameson and Caughey.[1-3] That method provides a discrete approximation to the nonlinear potential equation of transonic flow which may be interpreted either as a finite-difference method which balances fluxes across cell faces or as a finite element method based upon the Bateman variational principle. In the original formulation of that method, a first-order truncation error was introduced by the addition of an artificial viscosity needed to stabilize the scheme in regions of supersonic flow, and the difference equations were solved by an SLOR scheme.

A. Finite-Volume Formulation

Many aerodynamic problems of practical interest, including transonic flows with weak shock waves, can be usefully approximated as potential and steady. In strong conservation form, the equation for the velocity potential ϕ can be written in Cartesian coordinates (x,y,z) as

$$(\rho\phi_x)_x + (\rho\phi_y)_y + (\rho\phi_z)_z = 0, \qquad (1)$$

---
[1]Associate Professor, Sibley School of Mechanical and Aerospace Engineering. Member, AIAA.

where ρ is the density, given by the isentropic law

$$\rho = \{1 + (\gamma-1)/2 \ M_\infty^2 (1 - q^2)\}^{1/(\gamma-1)} \quad (2)$$

Here M_∞ is the Mach number of the free stream, q is the magnitude of the velocity $\nabla\Phi$, and the density and velocity have been normalized by their freestream values.

The finite-volume method for transonic potential flow[1-3] is a geometrically-general technique based upon a numerical evaluation of the transformation metrics produced by an arbitrary transformation to boundary-conforming coordinates. Consider a transformation to a new set of coordinates X,Y,Z. Let the Jacobian matrix of the transformation be defined by

$$H = \begin{Bmatrix} x_X & x_Y & x_Z \\ y_X & y_Y & y_Z \\ z_X & z_Y & z_Z \end{Bmatrix}, \quad (3)$$

and let h denote the determinant of H. The metric tensor of the new coordinate system is given by the matrix $G = H^T H$, and the contravariant components of the velocity vector U, V, and W are given by

$$\begin{Bmatrix} U \\ V \\ W \end{Bmatrix} = H^{-1} \begin{Bmatrix} u \\ v \\ w \end{Bmatrix} = G^{-1} \begin{Bmatrix} \Phi_X \\ \Phi_Y \\ \Phi_Z \end{Bmatrix}. \quad (4)$$

Eq.(1), upon multiplication by h, can then be written

$$(\rho h U)_X + (\rho h V)_Y + (\rho h W)_Z = 0. \quad (5)$$

The fully-conservative, finite-volume approximation corresponding to Eq.(5) is constructed by assuming separate trilinear variations of the independent and dependent variables within each mesh cell.
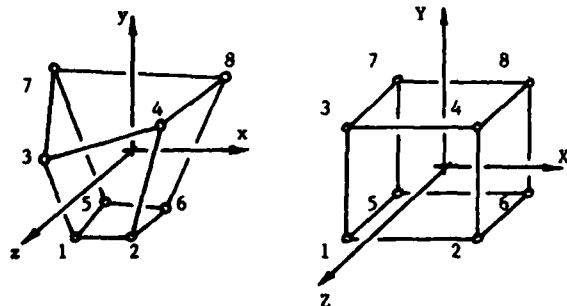
(a) Physical cell   (b) Computational cell

Figure 1.   Mapping of mesh cells.

Numbering the cell vertices as illustrated in Figure 1, and assuming that the local coordinates $X_i = \pm 1/2$, $Y_i = \pm 1/2$, $Z_i = \pm 1/2$ at the vertices, the local mapping can be written

$$x = 8 \sum_{i=1}^{4} x_i (1/4 + X_i X)(1/4 + Y_i Y)(1/4 + Z_i Z). \quad (6)$$

Similar formulas hold for y, z and Φ. If we introduce the averaging and differencing operators

$$\mu_X f_{i,j,k} = 1/2(f_{i+1/2,j,k} + f_{i-1/2,j,k})$$
$$\delta_X f_{i,j,k} = (f_{i+1/2,j,k} - f_{i-1/2,j,k}) \quad (7)$$

then the transformation derivatives, evaluated at the cell centers, can be expressed by formulas such as

$$x_X = \mu_{YZ} \delta_X x,$$
$$x_Y = \mu_{XZ} \delta_Y x, \quad (8)$$
$$x_Z = \mu_{XY} \delta_Z x,$$

with similar expressions for the derivatives of y, z and the potential. Such formulas can be used to determine ρ, h, U, V, and W at the center of each cell using Eqs.(2),(3), and (4). Eq.(5) is represented by conserving fluxes across the boundaries of auxiliary cells whose faces are chosen to be midway between the faces of the primary mesh cells. This can be represented as

$$\mu_{YZ} \delta_X (\rho h U) + \mu_{XZ} \delta_Y (\rho h V) + \mu_{XY} \delta_Z (\rho h W) = 0. \quad (9)$$

This formula can also be obtained by applying the Bateman variational principle that the integral of the pressure

$$I = \int p \ dx \ dy \ dz \quad (10)$$

is stationary, and approximating I by a simple one-point integration scheme in which the pressure at the center of each grid cell is multiplied by the cell volume. In this way, for subsonic flow, the finite-volume method can equally well be regarded as a finite element method with isoparametric trilinear elements.

The use of the one-point integration scheme leading to Eq.(9) has the advantage of requiring only one density evaluation per mesh point, but also has the undesirable effect of tending to decouple the solution at odd- and even-numbered points of the grid, and suitable recoupling terms can be added to improve the stability of the solution.

We define

$$T = -\frac{\epsilon}{2} \{ \mu_Z \delta_{XY} (A_X + A_Y) \mu_Z \delta_{XY}$$
$$+ \mu_X \delta_{YZ} (A_Y + A_Z) \mu_X \delta_{YZ} \quad (11)$$
$$+ \mu_Y \delta_{XZ} (A_X + A_Z) \mu_Y \delta_{XZ}$$
$$- 1/2 \delta_{XYZ} (A_X + A_Y + A_Z) \delta_{XYZ} \} \Phi,$$

where

$$A_X = \rho h(g^{11} - U^2/a^2),$$

$$A_Y = \rho h(g^{22} - V^2/a^2), \qquad (12)$$

$$A_Z = \rho h(g^{33} - W^2/a^2),$$

are the coefficients of ϕ_{XX}, ϕ_{YY}, and ϕ_{ZZ}, in the expanded form of Eq.(5). Here g^{ij} are the elements of the inverse of the metric tensor G^{-1}, and a^2 is the square of the local speed of sound. The addition of T to Eq.(5) provides recoupling for $0 \le \epsilon \le 1/2$. For $\epsilon = 1/2$, this reduces Eq.(9) to the usual second-order accurate, six-point Laplacian operator for incompressible flow on a uniform grid.

The scheme is stabilized in supersonic regions by the explicit addition of an artificial viscosity. The viscosity terms added in the original formulation are chosen to emulate the directional bias introduced by the rotated difference scheme of Jameson.[4] The fluxes $\hat{P}$, $\hat{Q}$, and $\hat{R}$ are defined such that

$$\hat{P}_{i,j,k} = \rho h \sigma/a^2(U^2\delta_{XX} + UV\delta_{XY} + UW\delta_{XZ})\phi,$$

$$\hat{Q}_{i,j,k} = \rho h \sigma/a^2(UV\delta_{XY} + V^2\delta_{YY} + VW\delta_{YZ})\phi, \quad (13)$$

$$\hat{R}_{i,j,k} = \rho h \sigma/a^2(UW\delta_{XZ} + VW\delta_{YZ} + W^2\delta_{ZZ})\phi,$$

where the switching function

$$\sigma = \max(0., 1 - (M_c/M)^2) \qquad (14)$$

is non-zero only for values of the local Mach number M greater than some critical Mach number M_c. Then, after defining

$$P_{i+1/2,j,k} = \begin{cases} \hat{P}_{i,j,k}, & U \ge 0, \\ -\hat{P}_{i+1,j,k}, & U < 0, \end{cases} \qquad (15)$$

with similar shifts for Q and R, Eq.(9) is represented as

$$\delta_X(\mu_{YZ}(\rho h U) + P) + \delta_Y(\mu_{XZ}(\rho h V) + Q)$$

$$+ \delta_Z(\mu_{XY}(\rho h W) + R) + T = 0. \qquad (16)$$

The difference Eqs.(9) approximate the original differential Eq.(5) to within a formal truncation error of second order in the mesh spacing in the physical plane when the mesh is smooth. Since the additional fluxes P, Q, and R added in supercritical regions are of the order of the physical mesh spacing itself, however, Eqs.(16) approximate Eq.(5) to within a truncation error of only first order in the mesh spacing. The error resulting from the introduction of the artificial viscosity can be reduced to second order nearly everywhere in the flow field if we define[6]

$$\nu_{i,j,k} = 1 - \kappa\delta_X\mu_{YZ}\rho \qquad (17)$$

where κ is a constant of order unity, and

$$P_{i+1/2,j,k} = \begin{cases} \hat{P}_{i,j,k} - \nu_{i,j,k}\hat{P}_{i-1,j,k}, & U \ge 0, \\ -\hat{P}_{i+1,j,k} + \nu_{i+1,j,k}\hat{P}_{i+2,j,k}. & U < 0, \end{cases} \qquad (18)$$

Similar expressions are used for the contributons from the Q and R fluxes. In regions where the solution is smooth, the term $\kappa\delta_X\mu_{YZ}\rho$ is of first order in the mesh spacing, and the viscosity is formally a second order quantity. Near a shock, for an appropriate value of κ, the quantity $\nu_{i,j,k}$ becomes small, and Eqs.(18) approximate Eqs.(15) -- i.e., the viscosity reverts to the original first-order form. This hybridization of the second-order scheme has been found necessary to stabilize computations for solutions containing strong shocks.

B. Multi-Grid Iteration

The difference equations resulting from Eq.(16) can be solved by carefully constructed SLOR schemes. The SLOR schemes described in References 1-3 were constructed in a manner that required only tridiagonal inversions along each line. When the contributions arising from the inclusion of the artificial viscosity terms are included, the corrections at each point are coupled to those of its two neighbors on one side (either side must be allowed in a general scheme, depending upon the sign of the velocity) for the first-order scheme, and its three nearest neighbors on one side for the second-order form of the viscosity. Thus, a general scheme which accounts for all these contributions would require a pentadiagonal inversion for the first-order scheme, or a septadiagonal inversion for the second-order scheme. It was found that the pentadiagonal inversion scheme was substantially more stable than the tridiagonal scheme when the second-order form of the viscosity was used, but made little difference in convergence behavior when the first-order viscosity was used. Complementary experiments by A. Jameson of Princeton University have shown no consistent advantage in using septadiagonal inversions (over the pentadiagonal scheme) when the second-order viscosity is used. The pentadiagonal inversion scheme has been incorporated for the present calculations.

Both X-line and Y-line schemes have been implemented. Only the Y-line scheme will be described here; the X-line scheme can be similarly constructed. Also, the coefficients will be described only for the case when $U,V,W > 0$; the coefficients for other cases can easily be constructed by analogy.

We define

$$A_U = \omega_s \rho h U/a^2 \max(|U|,|V|,|W|),$$

$$A_V = \omega_s \rho h V/a^2 \max(|U|,|V|,|W|), \qquad (19)$$

$$A_W = \omega_s \rho h W/a^2 \max(|U|,|V|,|W|),$$

where ω_s is a parameter governing the amount of ϕ_{st} type damping added explicitly to the time

3

dependent equation modelling the relaxation process. Also,

$$A_{UU} = \rho h \sigma U^2/a^2,$$

$$A_{VV} = \rho h \sigma V^2/a^2, \qquad (20)$$

$$A_{WW} = \rho h \sigma W^2/a^2.$$

Then the correction to the potential

$$C_{i,j,k} = \phi_{i,j,k}^{(n+1)} - \phi_{i,j,k}^{(n)}, \qquad (21)$$

is calculated according to

$$
\begin{aligned}
&(A_Y + A_V)(C_{i,j,k} - C_{i,j-1,k}) \\
&+ (A_Z + A_W)(C_{i,j,k} - C_{i,j,k-1}) \\
&+ (A_X + A_U)(C_{i,j,k} - C_{i-1,j,k}) \\
&\quad + A_X (C_{i,j,k} - C_{i+1,j,k}) \\
&+ A_{UU}\{-C_{i+1,j,k} + (3 + \nu_{i,j,k})C_{i,j,k} \qquad (22) \\
&\quad - (3 + 2\nu_{i,j,k} + \nu_{i-1,j,k})C_{i-1,j,k} \\
&\quad + (1 + \nu_{i,j,k} + \nu_{i-1,j,k})C_{i-2,j,k}\} \\
&+ A_{VV}\{(3 + \nu_{i,j,k})C_{i,j,k} - (4 + 3\nu_{i,j,k})C_{i,j-1,k} \\
&\quad + (1 + 2\nu_{i,j,k})C_{i,j-2,k}\} \\
&+ A_{WW}\{(3 + \nu_{i,j,k})C_{i,j,k} - (3 + \nu_{i,j,k})C_{i,j,k-1}\} \\
&\quad + (2/\omega - 1)(A_Y + A_Z)C_{i,j,k} = -R_{i,j,k}
\end{aligned}
$$

where $R_{i,j,k}$ is the residual of Eq.(16), calculated using values of the potential from the previous iteration, and ω is an overrelaxation parameter, which is set to 2 in supersonic regions. Eq.(22) requires a pentadiagonal inversion along each i-line since for $U < 0$ the formula must be modified to include the effect of the correction at the (i+2,j,k) point. The V and W components should be non-negative in supersonic zones for the relaxation sweeps to proceed in the positive Y- and Z- directions. Note that the influence of corrections at the (i,j+1,k) and (i,j,k+1), (i,j,k-2) points as well as the (i-3,j,k), (i,j-3,k) and (i,j,k-3) points have been eliminated by the effective addition of mixed space-time differences.

These SLOR schemes have the advantages of being quite stable, and of rapidly eliminating any large local errors in the initial estimates for the potential field. Their rates of convergence decrease as the local errors become smaller, however, with the result that convergence to very small residuals can be excruciatingly slow, especially when the mesh spacing is small.

An efficient alternative has been demonstrated by Jameson,[6] based upon the multi-level adaptive-grid technique first proposed by Fedorenko,[4] and developed and popularized by Brandt.[5] The concept behind the multi-grid method is to eliminate each band of wavenumbers in the error spectrum on a finite-difference grid which is, in a sense, optimal for that component. Thus, low wavenumber errors are eliminated on coarse grids, and only the high wavenumber components need be eliminated on the fine grids. Alternatively, the use of coarse grids to eliminate the low wavenumber component of the error can be thought of as allowing a very high signal speed for the effects of this error to be transmitted across the grid.

The multi-grid method was first applied to the transonic small disturbance equation by South and Brandt,[9] who noted the problems associated with highly stretched grids when using SLOR as the smoothing algorithm, and suggested using alternating SLOR as a remedy. Three-dimensional calculations using the full potential equation (in non-conservation form) have been performed by McCarthy and Reyhner,[10] for the transonic flow past axisymmetric inlets. Their computations were performed in a non-body-aligned, cylindrical coordinate system.

The structure of the multi-grid method is as follows. Let the discretization of Eq.(16) be represented by

$$L^k \phi^{(n+1)} = F^k, \qquad k = 1,2,\ldots,K, \qquad (23)$$

on a heirarchy of grid levels $G^0, G^1, \ldots, G^K$, with K denoting the finest grid. The iterative solution is started from some initial estimate on the finest grid. After the high wavenumber component of the error has been eliminated, the fine-grid residual is calculated and restricted to the next coarsest grid. On all but the finest grid, the residual must be modified to account for the difference in truncation error on the various grid levels (i.e., $L^k \phi \neq 0$ unless $k = K$, where ϕ is the converged solution on the K-th grid). Thus

$$F^{k-1} = L^{k-1}\phi^{(n)} - I_k^{k-1}L^k\phi^{(n)}, \qquad (24)$$

where I_k^{k-1} is a restriction operator which averages the residuals over the fine mesh points in the vicinity of each coarse grid point. After the high wavenumber error on the coarser grid has been eliminated, the finer mesh solution can be improved according to

$$\phi^{(n+1)} = \phi^{(n)} + I_{k-1}^k(\phi^{(n+1)} - \phi^{(n)}), \qquad (25)$$

where I_{k-1}^k is a prolongation operator which is used to interpolate the coarse grid corrections onto the finer grid.

While the essence of the idea has been described above for two grid levels, the idea can be extended to as many levels as feasible in order to work on the broadest possible band of the error wavenumber spectrum. Useful error reduction can be achieved on very coarse grids, containing only a few cells in each coordinate direction.

In the original implementation of Brandt,[5] an adaptive strategy was envisioned for determining when to change from one grid level to the next. The smoothing would continue on a particular grid level until the convergence rate fell below some predetermined tolerance, at which time the residual from that grid would be restricted to the next coarsest grid. The smoothing on that grid would proceed until the convergence rate again slowed, at which time the residual would again be restricted to a coarser grid, and the process repeated. When the solution had converged on the coarsest level, the corrections would successively be added back to the finer grid solutions, and the cycle would be repeated. In the present implementation, a simple fixed strategy has been found effective. A fixed number of relaxation sweeps is performed on each grid before restricting the residual from that grid to the next coarsest level, and a fixed number of relaxation sweeps is performed on each grid after the corrections are added from the preceding grid before the corrections are added to the next finest grid.

In the present codes, as in our earlier work,[8] the restriction operator averages the residuals at the 27 fine grid neighbors of each coarse grid point, weighted according to the fraction of the coarse grid cell volume asociated with each fine grid cell in the computational space. The prolongation operator uses four-point Lagrangian interpolation in each coordinate direction, except near boundaries where the order must be reduced.

The computational labor required for one multi-grid cycle using this fixed strategy is as follows. Let one work unit be defined as the labor required for one relaxation sweep on the finest grid. Then if m_1 sweeps are done on each grid before the residual is restricted to the next coarsest grid, and m_2 sweeps are done on each grid before the corrections are prolonged to the next finest grid, then the cost of one complete multi-grid cycle is approximately

$$\{8(m_1 + 1) + m_2\}/7 \text{ work units.}$$

This includes the cost of computing the residual on each grid for restriction to the next coarsest grid as approximately equal that of a relaxation sweep on that grid (since most of the labor is involved in computing the residual, not in the actual update of the solution), but neglects the overhead in restricting residuals and prolonging corrections. For $m_1 = m_2 = 1$, one multi-grid cycle requires approximately 2-3/7 work units.

The success of the multiple-grid method depends upon the efficient elimination of high wavenumber errors on any given grid. Jameson[6] used a generalized alternating-direction scheme, in which he replaced the usual constant in each factor by the sum of a constant and first-order difference operators in each coordinate direction. Shmilovich and Caughey[8] have shown that, even for SLOR schemes, the growth factor in a von Neumann analysis should never exceed approximately 0.78 per multi-grid cycle if the multi-grid algorithm is effective on error with low wavenumber components in any of the three coordinate directions. The effectiveness of the multi-grid procedure in eliminating error having low wavenumber component in only one (or two) directions was not verified in the present work, but it was found effective to alternate between X-line and Y-line SLOR in conjunction with the multi-grid procedure. This can be done in two different ways: (1) alternate multi-grid cycles can be performed using the two schemes, or (2) the two schemes can be alternated at each level within each multi-grid cycle (if m_1 and m_2 are greater than one). The most effective procedure seems to be the second option (with $m_1 = 2$ and $m_2 = 4$ or 6).

C. Geometrical Aspects

The algorithm described above has been incorporated into two computer programs for calculating the transonic potential flow past three-dimensional wings and wing-fuselage combinations. These codes are known generally as FLO-27 and FLO-30. FLO-27 analyses the flow past swept wings of essentially arbitrary planform and section shape; FLO-30 analyses the flow past such wings mounted upon arbitrary fuselage shapes.

Both codes construct boundary-conforming coordinate grids by sequences of simple conformal and shearing transformations. The computational domain in each program is terminated at artificial boundaries, located approximately ten chords distant from the wing surface in each spanwise surface, and approximately four semi-spans from the symmetry plane or fuselage in the lateral direction. On the upstream and lateral boundaries, the potential describing perturbations from the uniform free stream is set to zero, while on the downstream boundary, the velocity perturbations in the streamwise direction are set to zero (consistent with a fully-developed flow in the Trefftz plane). The no-flux condition is enforced directly in the flux balances at solid boundaries, and a linearized approximation to the vortex sheet, which assumes the shed vorticity trails in the freestream direction in a fixed surface downstream of the trailing edge is used. The flux balance represented by Eq.(16) is also satisfied at points on the vortex sheet, since it does not require differences across the sheet.

These codes, and their associated grid generation techniques, are described in greater detail in References 1-3.

III. RESULTS

Results will be presented illustrating both the improved rate of convergence of the multi-grid algorithm, and the increased accuracy of the scheme with the second-order viscosity.

A. Computational Aspects

Both programs have been designed to run on either modest computers with large virtual memory or on advanced machines with large high-speed memories. Even so, only the Cartesian

5

coordinates of the mesh and the solution vector can reasonably be stored for fine meshes, and the transformation derivatives are recomputed at each mesh point in each iteration. Largely because of this, the program runs efficiently on vector machines even though the actual line inversions for the solution are inherently recursive. On a grid containing 160x24x32 mesh cells in the X, Y, and Z directions, respectively, FLO-30 requires about 830,000 words of storage on the Cray-I computer, and requires about 2.0 CPU seconds per work unit on this grid. This corresponds to an estimated average computational rate of 32 megaflops. A typical solution is converged to within reasonable engineering accuracy after about 30 work units; this requires approximately 65 seconds on this (relatively fine) grid.

B. Computed Results

The first results to be presented are for the high-aspect-ratio, supercritical wing (Wing A) tested by Hinson and Burdges.[11] A perspective view of the wing is shown in Figure 2. The flow past the wing at a freestream Mach number of 0.82 and 1.5 degrees angle of attack was analysed using FLO-27. The analysis was performed on a sequence of three grids, each obtained by doubling the number of mesh cells in each coordinate direction from the preceding grid, and prolonging the results of the converged solution from the preceding grid as the initial estimate on the next grid. The finest grid contained 128x16x32 mesh cells. Calculations were performed with both the first- and second-order forms of the artificial viscosity; the iterative convergence rates were nearly identical. Figure 3 shows the convergence history of the second-order scheme on the finest grid. The logarithm of the average residual, the root section lift coefficient, and the number of supersonic points are plotted as a function of computational work (measured in work units); the lift coefficient is normalized by its final converged value, and number of super-sonic points is normalized by twice its final converged value, while the residual is normalized by its initial value. The solid lines represent the convergence of the multi-grid algorithm (with $m_1 = 2$, $m_2 = 6$, and the alternating SLOR scheme) using 4 grid levels, and the dashed lines represent the convergence of a relaxation solution for the same initial guess. Note that after even 100 relaxation sweeps, the SLOR scheme has eliminated only about half of the error in root section lift coefficient and in the number of super-sonic points. This illustrates the slowness with which SLOR eliminates the low wavenumber component of error. With the multi-grid scheme, both of these measures have converged to within the plottable accuracy of the figure in the equivalent of 50 relaxation sweeps. The wing surface pressure distribution for the first- and second-order accurate schemes are presented in Figures 4(a) and 4(b), and the streamwise pressure distributions at the 25 per cent semi-span station are presented for both schemes in Figures 5(a) and 5(b). Note the increased sharpness with which the shocks are resolved by the higher-order scheme. Finally, a convergence study of the wing lift and drag coefficients with mesh spacing is

shown in Figure 6. Both first- and second-order accurate results are plotted; the former vs. mesh spacing and the latter vs. the square of the mesh spacing. Straight lines through the finer mesh results for both schemes converge to the same asymptotic value for the lift coefficient in the limit of zero mesh width, but the drag results have not yet reached their asymptotic rates on these grids. The absolute error in lift for the second-order scheme on the finest grid is about 2 per cent, while a mesh containing more than eight times as many cells (a factor of 2 in each coordinate direction) would be required for similar accuracy using the first-order scheme. The absolute error in the drag coefficient for the second-order scheme is about 3 per cent, while similar accuracy for using the first-order scheme would seem to require approximately 64 times as many mesh cells (a factor of four in each coordinate direction).

Finally, to illustrate the reliability of the scheme, results for a strongly supercritical case are presented. The flow past the ONERA M-6 wing,[12] mounted upon a circular cylinder, was computed using FLO-30. Figure 7 shows the coordinate lines in the wing and fuselage surfaces for the grid used; only every fourth line is shown for clarity. The solution was computed at a freestream Mach number of 0.923 and 3.06 degrees angle of attack on a very fine grid containing 160x24x32 mesh cells. Nearly 20 per cent of the mesh points have supersonic velocities for this case. The wing pressure distribution, showing the strong shocks at the trailing edge of the upper surface and the substantial supersonic pocket outboard on the lower surface, is plotted in Figure 8. The convergence history is plotted in Figure 9. Again, the root section lift coefficient and the number of supersonic points have converged to within plottable accuracy in the equivalent of about 50 relaxation sweeps.

IV. CONCLUDING REMARKS

A multi-grid algorithm has been combined with a successive-line-overrelaxation (SLOR) iterative scheme to provide improved rates of convergence in the iterative sense for the computation of transonic potential flows past swept wing and wing-fuselage configurations. At the same time, a modified form of artificial viscosity has been incorporated which results in second-order accuracy for the scheme nearly everywhere in the flow field. The method has been incorporated into two computer programs for calculating the transonic potential flow past three-dimensional wings and wing-fuselage combinations. Results indicate that convergence adequate for most engineering purposes can be achieved with the new multi-grid algorithm in less than the time required for about 50 relaxation sweeps using the original SLOR scheme.

V. ACKNOWLEDGEMENTS

VI. REFERENCES

1. Jameson, Antony and Caughey, D.A., "A Finite-
Volume Method for Transonic Potential Flow Cal-
culations," Proc. of AIAA 3rd Computational Fluid
Dynamics Conference, pp. 35-54, Albuquerque,
N.M., June 27-29, 1977.

2. Caughey, D.A. and Jameson, Antony, "Numerical
Calculation of Transonic Potential Flow about
Wing-Body Combinations," AIAA Journal Vol. 17,
pp. 175-181, February 1979.

3. Caughey, D.A. and Jameson, Antony, "Progress
in Finite-Volume Calculations for Wing-Fuselage
Combinations," AIAA Journal Vol. 18, pp. 1281-
1288, November 1980.

4. Fedorenko, R. P., "A Relaxation Method for
Solving Elliptic Difference Equations," USSR
Comput. Math. and Math. Phys. Vol. 1, pp. 1092-
1096, 1962.

5. Brandt, Achi, "Multi-Level Adaptive Grid Tech-
nique (MLAT) for Fast Numerical Solution to Boun-
dary Value Problems," Proc. Third Int'l. Conf. on
Numerical Methods in Fluid Mechanics," Paris,
1972, Vol. 1, pp.82-89, Springer, New York, 1973.

6. Caughey, D. A. and Jameson, Antony, "Basic
Advances in the Finite-Volume Method for Tran-
sonic Potential Flow Calculations," Proc. of
Symposium on Numerical and Physical Aspects of
Aerodynamic Flows, Long Beach, California,
January 1981.

7. Jameson, Antony, "A Multi-Grid Scheme for
Transonic Potential Calculations on Arbitrary
Grids," Proc. of AIAA 4th Computational Fluid
Dynamics Conference, pp. 122-146, Williamsburg,
Va., July 23-25, 1979.

8. Shmilovich, A. and Caughey, D. A., "Applica-
tion of the Multi-grid Method to Calculations of
Transonic Potential Flow about Wing-fuselage
Combinations," Proc. of NASA Symposium on Multi-
grid Methods, NASA Ames Research Center, Moffett
Field, California, October 21-22, 1981, NASA CP
2202, pp. 101-130.

9. South, J. C. Jr., and Brandt, Achi, "Applica-
tion of a Multi-level Grid Method to Transonic
Flow Calculations," in Transonic Flow Problems in
Turbomachinery, pp. 180-207, T. C. Adamson and
M. F. Platzer, Eds. Hemisphere, Washington,
D. C., 1977.

10. McCarthy, D. R. and Reyhner, T. A., "Multi-
Grid Code for Three-dimensional Transonic Poten-
tial Flow about Inlets," AIAA Journal Vol. 20,
pp. 45-50, January 1980.

11. Hinson, B. L., and Burdges, K. P., "An Eval-
uation of Three-dimensional Transonic Codes using
New Correlation-tailored Test Data," AIAA Paper
80-0003, 13th Aerospace Sciences Meeting, Pasa-
dena, California, January 14-16, 1980.

12. Monnerie, B., et Charpin, F., "Essais de
buffeting d'une aile en fleche en transsonique,"
10e Colloque d'Aerodynamique Applique, Lille,
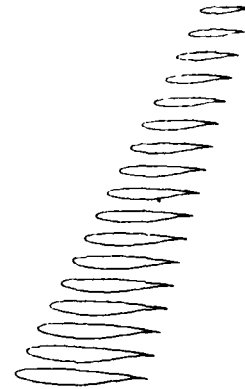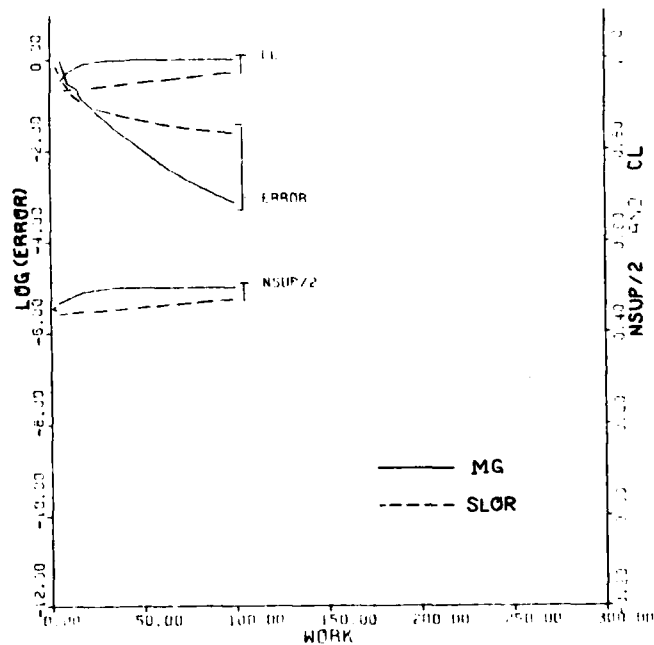France, November 1973.

Figure 2. Geometry of Lockheed Wing A; sections
at computational stations on fine grid are shown.

LOCKHEED WING A

MACH	0.820	ALPHA	1.500
RESID1	0.7890-05	RESID2	0.5340-08
WORK	100.47	RATE	0.9300
GRID	128X16X32		

Figure 3. Iterative convergence for calculation
of flow past Lockheed Wing A at $M_\infty = 0.82$ and
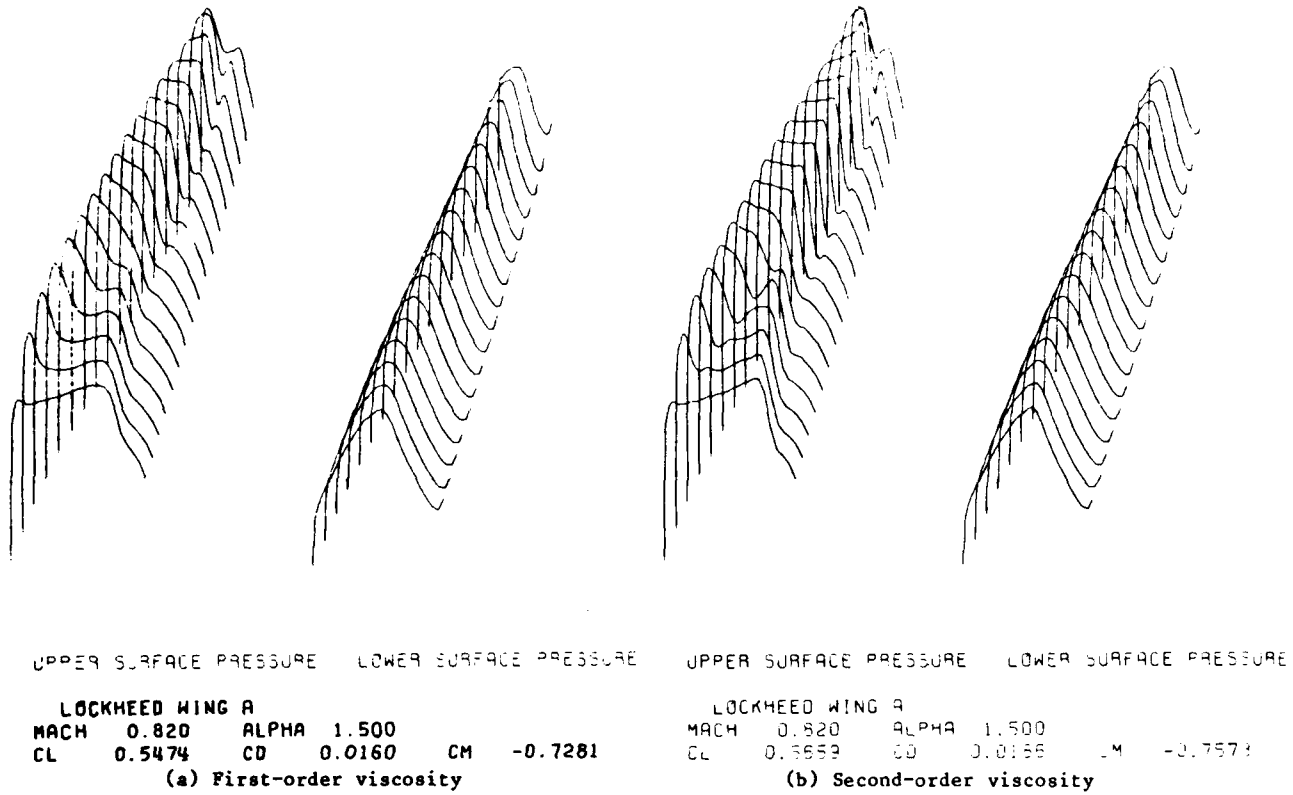1.5 degrees angle of attack; second-order
scheme.

UPPER SURFACE PRESSURE   LOWER SURFACE PRESSURE   UPPER SURFACE PRESSURE   LOWER SURFACE PRESSURE

LOCKHEED WING A   LOCKHEED WING A
MACH   0.820   ALPHA 1.500   MACH   0.820   ALPHA 1.500
CL   0.5474   CD   0.0160   CM   -0.7281   CL   0.5559   CD   0.0156   CM   -0.7573
            (a) First-order viscosity   (b) Second-order viscosity

Figure 4.   Three-dimensional wing surface pressure distributions for Lockheed
            Wing A at M_∞ = 0.82   and   1.5   degrees angle of attack.

LOCKHEED WING A   LOCKHEED WING A
MACH   0.820   ALPHA 1.500   ETA   0.250   MACH   0.820   ALPHA 1.500   ETA   0.250
CL   0.5364   CD   0.0212   CM   -0.2096   CL   0.5517   CD   0.0243   CM   -0.2183
            (a) First-order viscosity   (b) Second-order viscosity
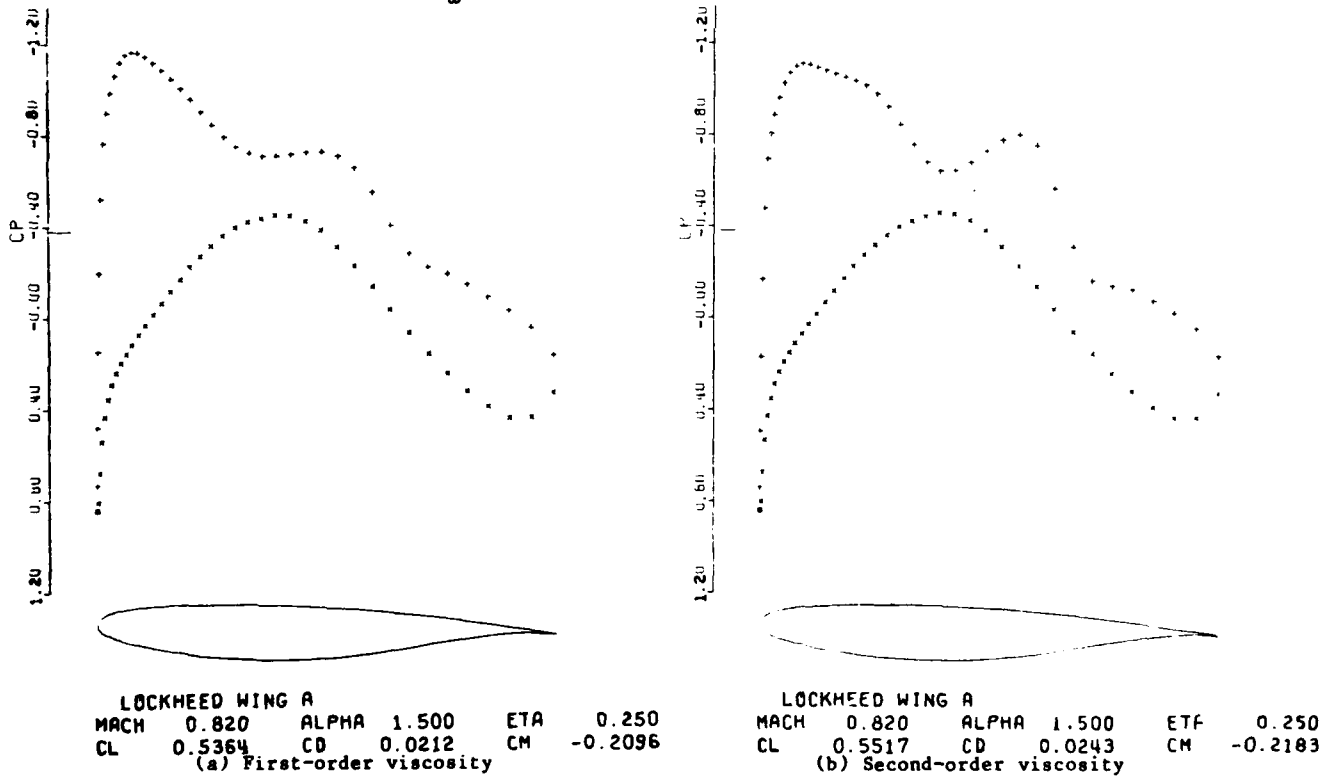
Figure 5.   Streamwise surface pressure distributions for Lockheed Wing A at 25
            per cent semi-span station.   Same freestream conditions as Figure 4.
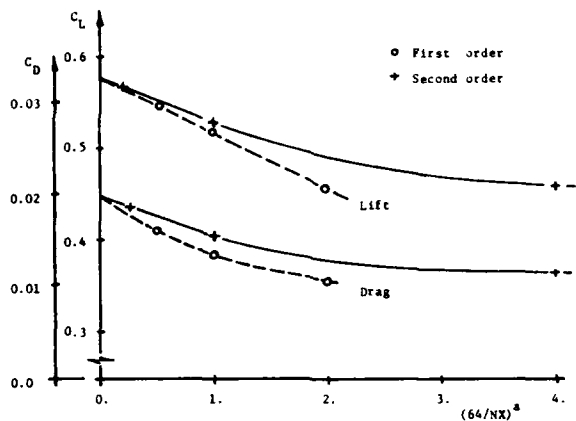
8

Figure 6. Convergence study of wing lift and drag coefficients for Lockheed Wing A. Same freestream conditions as Figures 4 and 5.
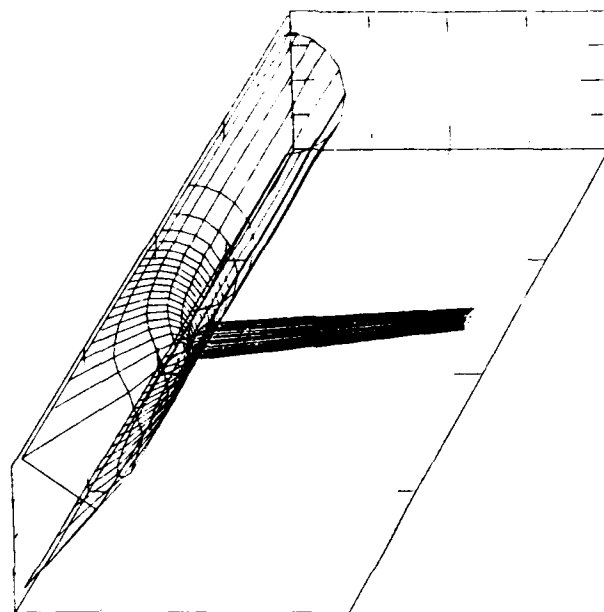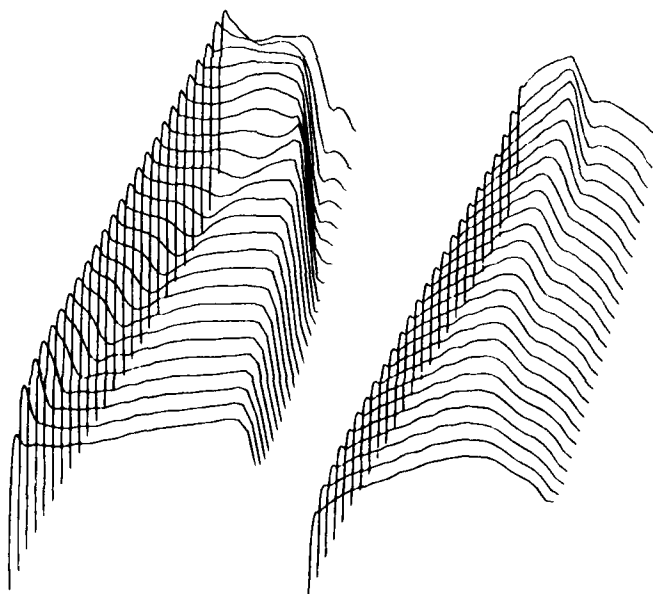

Figure 7. ONERA wing M-6 mounted upon cylindrical fuselage. Grid lines shown in wing and fuselage surfaces only; every fourth line shown.

UPPER SURFACE PRESSURE   LOWER SURFACE PRESSURE

ONERA WING ON CYLINDRICAL FUSELAGE
MACH   0.923   ALPHA   3.060
CL   0.4779   CD   0.0444   CM   -0.4543

Figure 8. Wing surface pressure distribution for flow past ONERA Wing-cylinder combination at $M_\infty = 0.923$ and 3.06 degrees angle of attack.
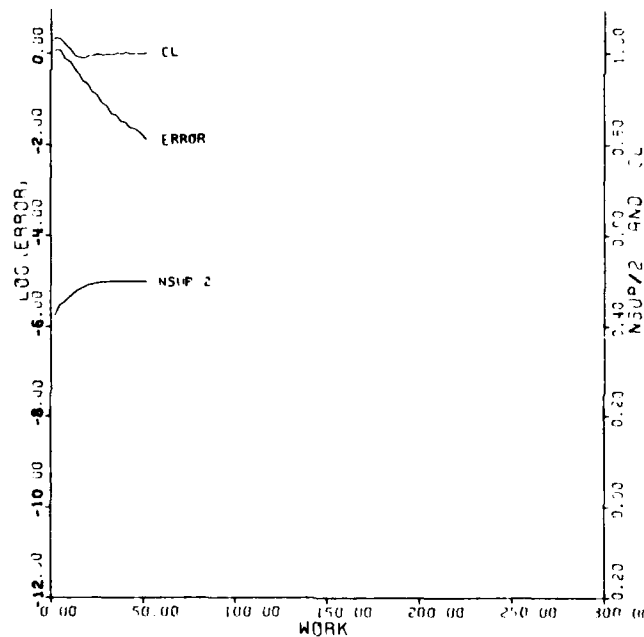
ONERA WING ON CYLINDRICAL FUSELAGE
MACH   0.923   ALPHA   3.060
RESID1 0.532D-04   RESID2 0.683D-06
WORK   52.37   RATE   0.9202
GRID   160X24X32

Figure 9. Iterative convergence for calculation of flow past ONERA wing-cylinder combination. Freestream conditions as in Figure 8.

END

FILMED

10-83

DTIC